First-Principles Prediction of Ultralow Lattice Thermal Conductivity of Dumbbell Silicene: A Comparison with Low-Buckled Silicene

Bo Peng,[†] Hao Zhang,[*,†] Hezhu Shao,[‡] Yuanfeng Xu,[†] Rongjun Zhang,[†] Hongliang Lu,[¶] David Wei Zhang,[¶] and Heyuan Zhu[*,†]

[†]Shanghai Ultra-precision Optical Manufacturing Engineering Research Center and Key Laboratory of Micro and Nano Photonic Structures (Ministry of Education), Department of Optical Science and Engineering, Fudan University, Shanghai 200433, China

[‡]Ningbo Institute of Materials Technology and Engineering, Chinese Academy of Sciences, Ningbo 315201, China

[¶]State Key Laboratory of ASIC and System, Institute of Advanced Nanodevices, School of Microelectronics, Fudan University, Shanghai 200433, China

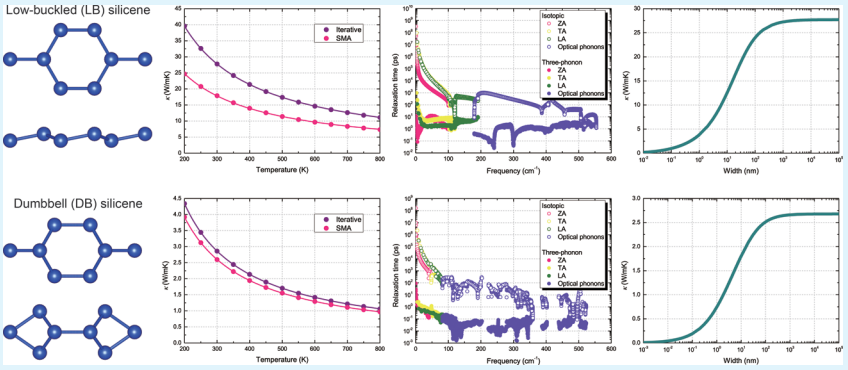

ABSTRACT: The dumbbell structure of two-dimensional group IV material offers alternatives to grow thin films for diverse applications. Thermal properties are important for these applications. We obtain the lattice thermal conductivity of low-buckled (LB) and dumbbell (DB) silicene by using first-principles calculations and the Boltzmann transport equation for phonons. For LB silicene, the calculated lattice thermal conductivity with naturally occurring isotope concentrations is 27.72 W/mK. For DB silicene, the calculated value is 2.86 W/mK. The thermal conductivity for DB silicene is much lower than LB silicene due to stronger phonon scattering. Our results will induce further theoretical and experimental investigations on the thermoelectric (TE) properties of DB silicene. The size-dependent thermal conductivity in both LB and DB silicene is investigated as well for designing TE devices. This work sheds light on the manipulation of phonon transport in two-dimensional group IV materials by dumbbell structure formed from the addition of adatoms.

KEYWORDS: *2D group IV materials, silicene, phonon transport, dumbbell structure, Boltzmann transport equation*

1. INTRODUCTION

Unique electronic properties, high chemical stability, and mechanical strength have made graphene a material of interest in various fields ranging from electronics to energy conversion devices.[1−7] Reasonably, other group IV elements have been considered as candidates to have a graphenelike two-dimensional (2D) honeycomb structure with similar exceptional properties.[8−18] Recently, silicene, germanene, and stanene (2D silicon, germanium, and tin nanosheet, respectively) have been fabricated by epitaxial growth on substrates.[19−21] Compared to other 2D group IV materials, the realization of silicene would be of great importance because of its easier incorporation into silicon-based microelectronics industry. First-principles calculations have predicted that silicene has a low-buckled (LB) honeycomb structures.[8,14] However, to explain some characteristics of silicene grown on Ag(111) surfaces, some modifications of this graphene-like structure have been proposed: the addition of Si adatoms to LB silicene results in the formation of a dumbbell (DB) structure with a lower total energy per atom.[16,22−24] These works enrich the family of 2D group IV materials beyond the LB honeycomb lattices. Furthermore, DB structures occur not only for monolayer monatomic honeycomb structures, but also for their compounds such as SiGe and SiC.[16,22−30] For the formation of DB structures, the energy barrier is not high, which can offer alternatives to grow thin films with diverse properties.[24] Although the electronic, optical, and magnetic properties of DB silicene have been studied intensively,[16,22−24] the phonon transport properties, which play an important role in potential applications such as electronic and energy conversion devices, are not revealed.

For application in thermoelectric (TE) energy conversion, it is important to reduce the lattice thermal conductivity of a

material while maintaining a high electrical conductivity, which often conflict with each other.[31,32] Traditionally there are four factors to guide the search for low thermal conductivity materials: (1) weak interatomic bonding, (2) high average atomic mass, (3) complex crystal structure, and (4) high anharmonicity.[33] According to Slack's theory, weak interatomic bonding and high average atomic mass imply a low Debye temperature, and high anharmonicity indicates strong anharmonic phonon scattering, which lead to a low thermal conductivity. This has been observed in Cu_2GeSe_3 and monolayer transition metal dichalcogenides (MoS_2, $MoSe_2$ and WS_2) in our previous work.[34,35] Fully microscopic computational materials techniques have been developed to study thermal transport properties recently.[36−39] Thus, systematic investigations of phonon transport properties in LB and DB silicene can be performed.

Here we investigate the lattice thermal conductivity κ of both LB and DB silicene using first-principles calculations and self-consistent iterative solution of the Boltzmann transport equation (BTE) for phonons.[37−39] A much lower thermal conductivity in DB silicene is observed (2.86 W/mK), which may indicate higher TE efficiency and will induce further investigations on the TE performance of DB silicene. The underlying mechanism is investigated by both Slack's theory and calculation of phonon relaxation time. The influence of naturally occurring isotopes is studied as well. Finally, for designing TE nanostructures, we investigate the size-dependent lattice thermal conductivity.

2. METHODOLOGY

The in-plane κ is isotropic and can be calculated as[40,41]

$$\kappa = \kappa_{\alpha\alpha} = \frac{1}{V}\sum_{\lambda} C_\lambda v_{\lambda\alpha}^2 \tau_{\lambda\alpha} \quad (1)$$

where V is the crystal volume, λ is the phonon mode (comprising both a wave vector $\mathbf{q}$ and a phonon branch index j), C_λ is the heat capacity per mode, $v_{\lambda\alpha}$ is the group velocity of mode λ along α direction, and $\tau_{\lambda\alpha}$ is the relaxation time. We use the nominal layer thicknesses h = 4.20 Å for both LB and DB silicene, corresponding to the van der Waals radii of silicon.[42,43] Using the ShengBTE code,[36−39] we calculate the lattice thermal conductivity iteratively with the harmonic and anharmonic (third-order) interatomic force constants (IFCs) as the only inputs, which are obtained from first-principles calculations.

We perform the calculations based on density functional theory (DFT) using the Vienna ab initio simulation package (VASP).[44] We choose the generalized gradient approximation (GGA) in the Perdew−Burke−Ernzerhof (PBE) parametrization for the exchange-correlation functional. A plane-wave basis set with kinetic energy cutoff of 600 eV is employed. During structural relaxation for the unit cell of LB (DB) silicene, a 21 × 21 × 1 (15 × 15 × 1) $\mathbf{q}$-mesh is used, until the energy differences are converged within 10^{-6} eV, with a Hellman-Feynman force convergence threshold of 10^{-2} eV/Å. A vacuum spacing larger than 15 Å (20 Å) is used for LB (DB) silicene to eliminate interactions between adjacent layers.

By calculating the dynamical matrix through the linear response of electron density, the harmonic IFCs can be obtained based on density functional perturbation theory (DFPT).[45] Using the supercell approach, a 5 × 5 × 1 (3 × 3 × 1) supercell with 5 × 5 × 1 (3 × 3 × 1) $\mathbf{q}$-mesh is used for LB (DB) silicene. The phonon dispersion relation is obtained using the harmonic IFCs, and subsequently the group velocity $v_{\lambda\alpha}$ and specific heat C_λ can be obtained. The third-order anharmonic IFCs play a significant role in determining the three-phonon scattering rate, which is the inverse of $\tau_{\lambda\alpha}$. Using a supercell-based, finite-difference method, the anharmonic IFCs are calculated,[39] and the same 5 × 5 × 1 (3 × 3 × 1) supercell is used for LB (DB) silicene with 5 × 5 × 1 (3 × 3 × 1) $\mathbf{q}$-mesh. We include the interactions with the eighth nearest-neighbor atoms for both structures, which is well converged.

The convergence of κ with respect to $\mathbf{q}$ points is tested in our calculation. We introduce discretizationa of the Brillouin zone (BZ) into a Γ-centered regular grid of 90 × 90 × 1 (50 × 50 × 1) $\mathbf{q}$ points for LB (DB) silicene. A Gaussian function is used to enforce the conservation of energy in the three-phonon processes with a scale parameter of 0.5 for broadening.[38]

3. RESULTS AND DISCUSSION

3.1. Crystal Structures and Phonon Dispersions. Figure 1 shows the optimized structure of LB and DB silicene. The

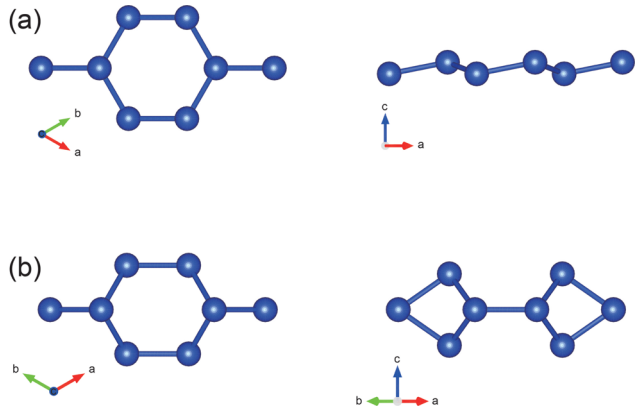

Figure 1. Top view and side view of (a) LB and (b) DB silicene.

optimized LB silicene has a hexagonal structure with space group $P\bar{3}m1$ and 2 Si atoms in one unit cell. A low-buckled configuration is found in Figure 1a, which is similar to LB germanene and stanene.[9,10,14,16,17] As shown in Figure 1b, the optimized DB silicene has a hexagonal structure with space group $P6/mmm$ and 10 Si atoms in one unit cell. Two DB units are formed at the para positions of a honeycomb ring and the other Si atoms stay in the same plane, which is similar to DB stanene and DB Sn_6Ge_4.[28,30] The optimized geometries of LB and DB silicene are listed in Table 1. The lattice constant a and

Table 1. Lattice Constant a, Buckling Height h, and Cohesive Energy E_c of LB and DB Silicene[a]

	a (Å)	h (Å)	E_c (eV/atom)
LB silicene	3.87	0.44	4.77
	(3.87[46])	(0.45[46])	(4.57[46])
	(3.87[47])	(0.44[47])	
	(3.88[14])	(0.44[14])	
DB silicene	7.43	2.71	4.98
	(7.43[16])	(2.71[16])	

[a]Other theoretical data are listed in parentheses for comparison.

buckling height h of both LB and DB silicene are in good agreement with previous studies.[14,16,46,47] In fact, when Si adatoms are placed on silicene, DB structures can be formed without any energy barrier,[25] and these adatoms gradually cover the surface uniformly.[24] The DB structures can construct stable periodic structures with higher cohesive energy, because DB-DB coupling is attractive until the first nearest-neighbor separation,[24,26] and the energy barrier to the migration of DBs along the straight path between the two first (second) nearest-neighbor atoms of silicene is 0.75 (0.95) eV.[24] As shown in Table 1, the calculated cohesive energy per Si atom

for DB silicene is 0.21 eV higher than that of LB silicene, indicating that DB silicene is more stable.

High cohesive energy may not ensure that these two materials correspond to deep minima in the Born–Oppenheimer surface. Here, we investigate the dynamic stability of these two structures by the calculations of phonon dispersion in Figure 2. The calculated phonon dispersion of LB

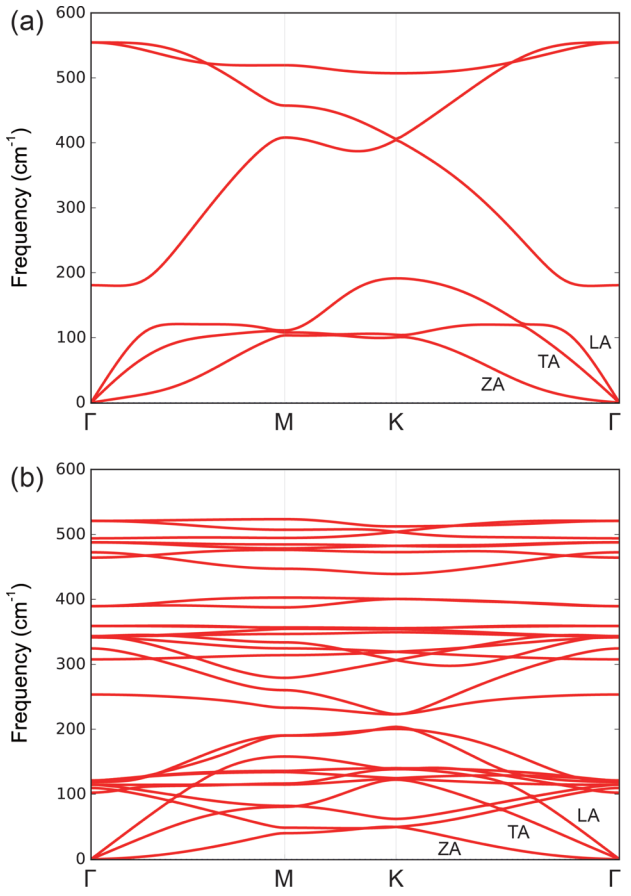

Figure 2. Phonon dispersion for (a) LB and (b) DB silicene along different symmetry lines.

silicene is in good agreement with previous works.[46−49] The frequencies of all modes are positive over the whole BZ, therefore both LB and DB silicene are dynamically stable.

As shown in Figure 2a, the longitudinal acoustic (LA) and transverse acoustic (TA) branches of LB silicene are linear near the Γ point, and out-of-plane acoustic (ZA) branch shows a quadratic trend with a linear component; while the ZA branch of DB silicene is totally quadratic near the Γ point, as shown in Figure 2b. This difference comes from the structural difference. DB silicene belongs to D_{6h} point group, whereas the buckled structure belongs to the point group symmetry of D_{3d}, which breaks the reflection symmetry, and therefore the Z modes of LB silicene couple with the XY modes.[48,49] This results in the linear dispersion component of ZA phonons near the Γ point. Similar linear ZA dispersion has been observed in other buckled structures such as germanene and stanene.[17,47,49]

The different shapes of ZA phonon dispersion lead to different group velocities v_g for LB and DB silicene near the zone center. As shown in Figure 3a, a small but nonzero sound velocity for the ZA branch of silicene is observed in LB silicene, which is consistent with other studies.[48,50] This is because the

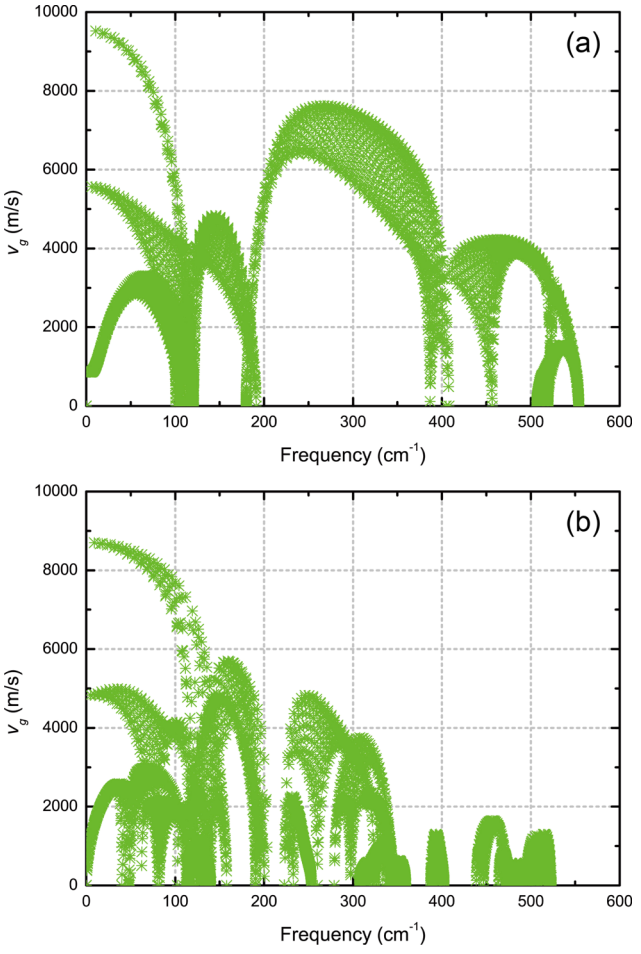

Figure 3. Calculated phonon group velocities v_g of (a) LB and (b) DB silicene in the whole BZ.

dispersion of the ZA branch near the Γ point contains a linear component. The phonon group velocities of LB and DB silicene for the ZA, TA, and LA modes in the long-wavelength are listed in Table 2. It should be noticed that the sound velocities of LB silicene for the ZA, TA, and LA modes are larger than those of DB silicene.

Table 2. Sound Velocities and Debye Temperature Θ_D of LB and DB Silicene in Comparison with Graphene

	v_g(ZA) (m/s)	v_g(TA) (m/s)	v_g(LA) (m/s)	Θ_D (K)
LB silicene	860	5570	9520	798.1
DB silicene	0	4850	8700	753.4
graphene	0	13 880[51]	22 000[51]	2300[52]

The Debye temperature Θ_D can be calculated with the maximum optical phonon frequency (Debye frequency) ω_m[53]

$$\Theta_D = h\omega_m/k_B \quad (2)$$

where h is the Planck constant and k_B is the Boltzmann constant. The calculated Θ_D values of LB and DB silicene are given in Table 2. Because the Debye temperature reflects the magnitude of sound velocity,[34] it is expected that the larger the sound velocities, the higher the Debye temperature.[54] The Debye temperature of LB silicene is higher than that of DB silicene, which is in consistency with the fact that the sound velocities of LB silicene are larger. For comparison, we also list

the phonon group velocities in the long-wavelength limit and Debye temperature of graphene in Table 2. The Θ_D of graphene is much higher than that of LB and DB silicene. The Debye temperature is a measure of the temperature above which all modes begin to be excited and below which modes begin to be frozen out.[55] Generally, low Θ_D corresponds to low thermal conductivity according to the aboved-mentioned Slack's theory,[33,35] because lower Debye temperature indicates smaller phonon velocities and lower acoustic-phonon frequencies, and low acoustic-phonon frequencies further increase phonon populations, which subsequently increase phonon scattering rates.[55−57]

The mode Grüneisen parameters provide information about the anharmonic interactions and can be calculated directly from the anharmonic IFCs[37]

$$\gamma_\lambda = -\frac{1}{6\omega_\lambda^2}\sum_{\eta' l'}\sum_{\eta'' l''}\sum_{\alpha\beta\gamma}\Phi^{\alpha\beta\gamma}_{\eta 0,\eta' l',\eta'' l''}\frac{e^j_{\alpha\eta}(\mathbf{q}^*)e^j_{\beta\eta'}(\mathbf{q})}{\sqrt{M_\eta M_{\eta'}}}e^{i\mathbf{q}\mathbf{R}^i}\mathbf{r}_{\eta'' l''\gamma} \quad (3)$$

where α, β, and γ are the Cartesian components, $\Phi^{\alpha\beta\gamma}_{\eta 0,\eta' l',\eta'' l''}$ is the third-order anharmonic IFCs, $e^j_{\alpha\eta}(\mathbf{q}^*)$ and $e^j_{\beta\eta'}(\mathbf{q})$ are the phonon eigenvectors, and $\mathbf{r}_{\eta'' l''\gamma}$ is the position of η^{th} atom in l^{th} primitive cell. Figure 4 shows the mode Grüneisen parameters within the whole BZ for LB and DB silicene. The Grüneisen parameters of DB silicene are larger than those of LB silicene at low frequencies, indicating higher anharmonicity of DB silicene. Therefore, DB silicene has much stronger anharmonic phonon scattering than LB silicene at low frequencies. These large mode Grüneisen parameters at low frequencies are crucial to the understanding of the phonon transport in DB silicene, because most of the heat is carried by low-frequency phonons.

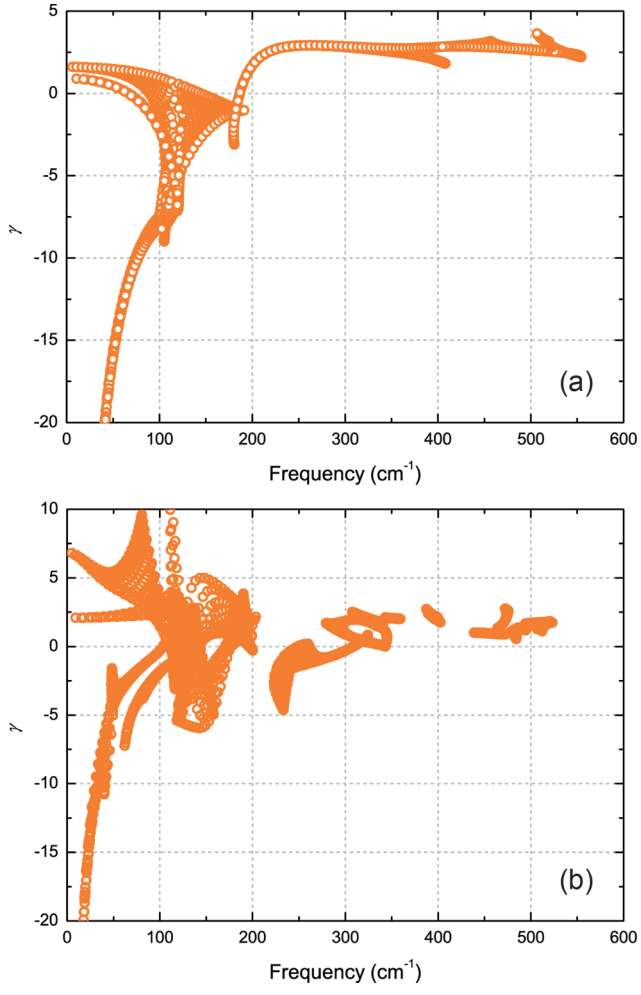

Figure 4. Calculated Grüneisen parameters for (a) LB and (b) DB silicene within the whole BZ.

3.2. Thermal Conductivity. The room-temperature lattice thermal conductivity of naturally occurring (κ_{nat}) and isotopically pure (κ_{pure}) silicene are listed in Table 3. The calculated thermal conductivity of free-standing LB silicene is in good agreement with other theoretical results.[48,58−60] Compared to LB silicene, much lower thermal conductivity is observed in DB silicene. It should be noticed that only free-standing silicene is considered here. However, in device applications, both LB and DB silicene are usually synthesized on various substrates, and as a result, the thermal conductivity will be further affected. In fact, for LB silicene, the influence of substrate on the thermal transport is in debate. Wang et al. have found that, in LB silicene, though the coupling of ZA modes to the substrate linearizes the phonon dispersion and increases the group velocity, the relaxation times of the ZA phonons are dramatically decreased, because the presence of the substrate breaks the reflection symmetry and introduces more phonon scattering.[61] Thus, the presence of a SiO_2 substrate results in a large reduction to the thermal conductivity at 300 K. However, from nonequilibrium molecular dynamics simulations, Zhang et al. have found that by changing the surface crystal plane of the substrate, the thermal conductivity of LB silicene can be either suppressed or enhanced.[62]

Table 3. κ_{nat}, κ_{pure}, P_3, and Contribution of ZA, TA, LA, and Optical Phonon Modes toward the κ_{nat} in All Studied 2D Group IV Crystals at 300 K

	κ_{nat} (W/mK)	κ_{pure} (W/mK)	P_3	ZA (%)	TA (%)	LA (%)	optical (%)
LB silicene	27.72	28.85	0.15	38.98	21.63	20.97	18.42
DB silicene	2.86	2.86	4.08	20.22	34.43	22.01	23.34

The reduced thermal conductivity in DB silicene can be explained by conventional Slack's theory. Lower Debye temperature in DB silicene results in decreased phonon velocities and higher phonon scattering rates since more phonon modes are active at a given temperature.[55,56] The crystal structure of DB silicene is more complex: there are 10 atoms in the unit cell of DB silicene, corresponding to 3 acoustic and 27 optical phonon branches, indicating that a phonon can be scattered more easily in DB silicene (more three-phonon groups that can satisfy the energy and quasi-momentum conservations). In addition, large mode Grüneisen paramters of DB silicene imply strong anharmonic phonon scattering as well. Consequently, the thermal conductivity of DB silicene is significantly reduced. Our results indicate that the lattice thermal conductivity of 2D group IV materials can be tuned by dumbbell structure formed from the addition of adatoms.

As present in Table 3, the thermal conductivity of LB and DB silicene are insensitive to the naturally occurring isotope, since the Umklapp processes become dominant over isotopic scattering at high temperatures and consequently drive the

thermal conductivity.[63,64] In addition, DB silicene has much stronger anharmonic phonon scattering as mentioned above. Therefore, the isotopic influence on thermal conductivity is much less obvious in DB silicene than in LB silicene.

Figure 5 presents the lattice thermal conductivity for LB and DB silicene with naturally occurring isotope concentrations as a

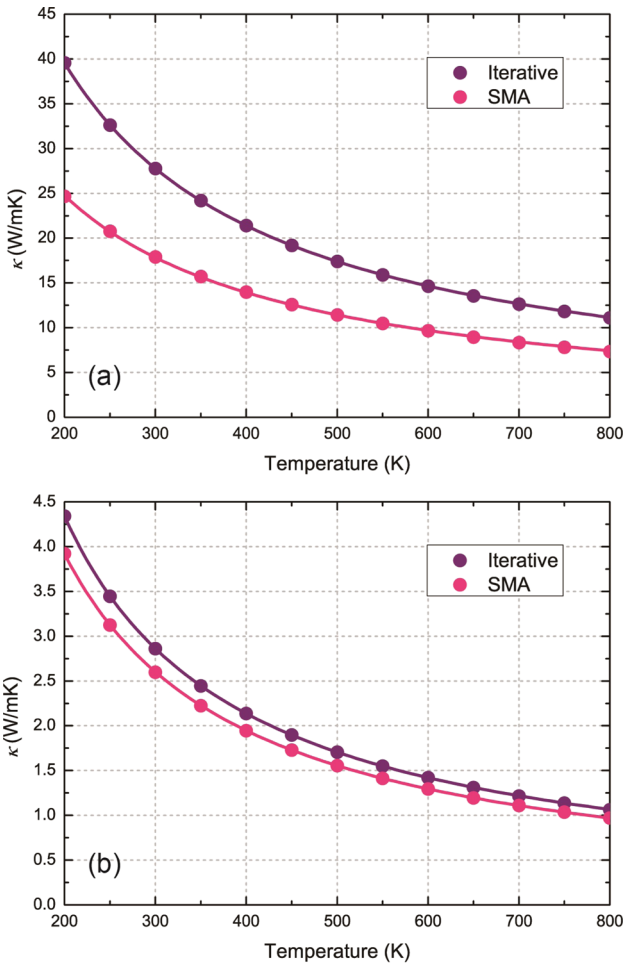

Figure 5. Thermal conductivity as a function of temperature for (a) LB and (b) DB silicene.

function of temperature. The thermal conductivity decreases with increasing temperature, as expected for a phonon-dominated crystalline materials. We also compare the thermal conductivity calculated from the iterative and single-mode relaxation time approximation (SMRTA) solution. The difference between the two approaches for DB silicene is much smaller than that for LB silicene. The SMRTA has no memory of the initial phonon distribution, because it assumes that phonons are excited individually. As a result, when the momentum-conserving Normal processes play an important role, the SMRTA typically does not work well.[65] Our results indicate the dominant role of the Umklapp processes in phonon−phonon interactions of DB silicene over a wide temperature range.

High TE performance requires the system to be a bad conductor for phonons. The ultralow lattice thermal conductivity of DB silicene (2.86W/mK at 300 K) is similar in magnitude to that of state-of-the-art TE materials such as PbTe (2.8 W/mK[66]) and Cu_2GeSe_3 (2.0−2.4 W/mK[34]). DB silicene may realize much higher thermoelectric efficiency considering the ultralow lattice thermal conductivity (2.86W/mK), which will induce further investigations on the performance of TE devices based on silicene. Compared to other 2D hexagonal materials, the lattice thermal conductivity of DB silicene is much lower than that of LB germanene (20.2 W/mK)[51] and stanene (11.6 to 26.2 W/mK),[17,51] monolayer MoS_2 (30−100 W/mK),[35,67−69] and blue phosphorene (78 W/mK),[70] whereas it is at least 3 orders of magnitude smaller than that of graphene (3000−5000 W/mK).[13,48,71] This is due to strong three-phonon scattering in DB silicene as we mentioned above.

To understand the underlying mechanism of low lattice thermal conductivity of DB silicene, the key physical insight can be obtained by calculating the allowed phase space for three-phonon processes P_3. In the temperature range where three-phonon processes are dominant, the total phase space for three-phonon processes P_3 is defined by[37,72]

$$P_3 = \frac{2}{3\Omega}\left(P_3^{(+)} + \frac{1}{2}P_3^{(-)}\right) \tag{4}$$

where Ω is a normalization factor,[73] and

$$P_3^{(\pm)} = \sum_j \int d\mathbf{q} D_j^{(\pm)}(\mathbf{q}) \tag{5}$$

and

$$D_j^{(\pm)}(\mathbf{q}) = \sum_{j',j''} \int d\mathbf{q}' \delta(\omega_j(\mathbf{q}) \pm \omega_{j'}(\mathbf{q}') - \omega_{j''}(\mathbf{q} \pm \mathbf{q}' - \mathbf{G})) \tag{6}$$

where $D_j^{+}(\mathbf{q})$ corresponds to absorption processes, i.e., $\omega_j(\mathbf{q})+\omega_{j'}(\mathbf{q}') = \omega_{j''}(\mathbf{q}+\mathbf{q}'-\mathbf{G})$, whereas $D_j^{-}(\mathbf{q})$ corresponds to emission processes, i.e., $\omega_j(\mathbf{q}) = \omega_{j'}(\mathbf{q}')+\omega_{j''}(\mathbf{q}-\mathbf{q}'-\mathbf{G})$. According to eqs 4−6, P_3 provides a measure of the phase space available for three-phonon processes of each phonon mode. Larger phase space for three-phonon processes usually implies a larger number of available scattering channels. Consequently, there is an inverse relationship between P_3 and the intrinsic lattice thermal conductivity of a material.[63,72] As shown in Table 3, DB silicene has larger P_3 than LB silicene, indicating a larger number of available scattering channels for phonons. This is consistent with the above analysis showing that the anharmonic phonon scattering in DB silicene is stronger.

Furthermore, the relaxation time of each phonon mode for LB and DB silicene is extracted to reveal the scattering mechanism in detail. Figure 6 presents the isotopic relaxation time and the intrinsic three-phonon relaxation time of each phonon mode for these two materials. Isotopic scattering processes are frequency-dependent. The low-frequency phonons can transport nearly all the heat with little isotopic scattering,[74] thus at low frequencies we observe the relative long isotopic relaxation time of acoustic phonons. The total scattering rate is a sum of contributions from isotopic scattering and anharmonic three-phonon scattering,[40,63]

$$1/\tau_j(\mathbf{q}) = 1/\tau_j(\mathbf{q})^{\text{iso}} + 1/\tau_j(\mathbf{q})^{\text{anh}} \tag{7}$$

The anharmonic three-phonon scattering is much stronger than isotopic scattering (corresponding to shorter relaxation time). Thus, with much shorter relaxation time, the three-phonon scattering dominates the total relaxation time.

As shown in Figure 6a, the three-phonon relaxation time of LB silicene agrees well with previous results.[60] It should be

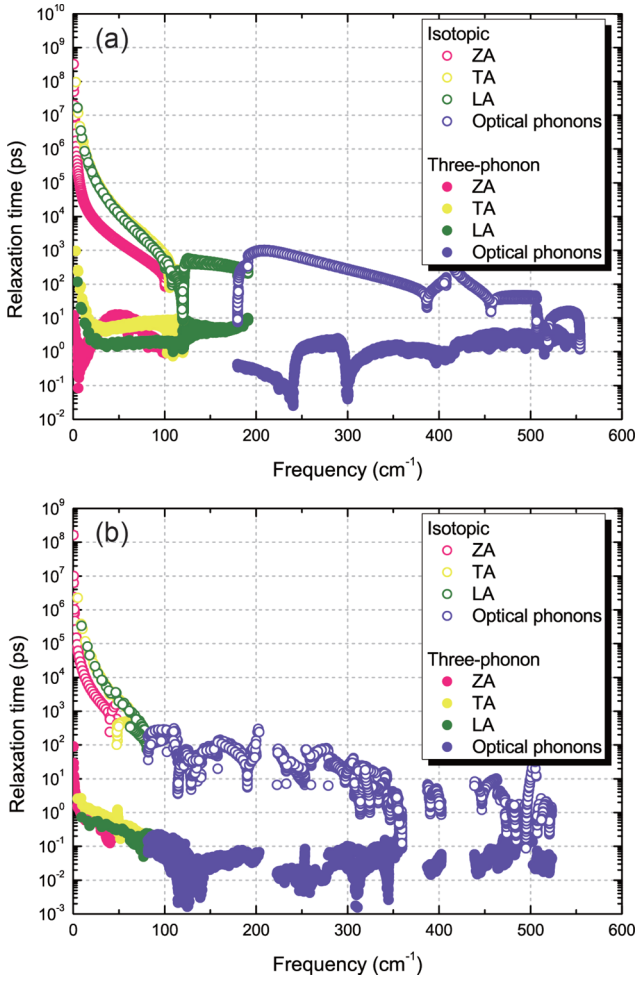

Figure 6. Isotopic and three-phonon relaxation time of each phonon mode for (a) LB and (b) DB silicene.

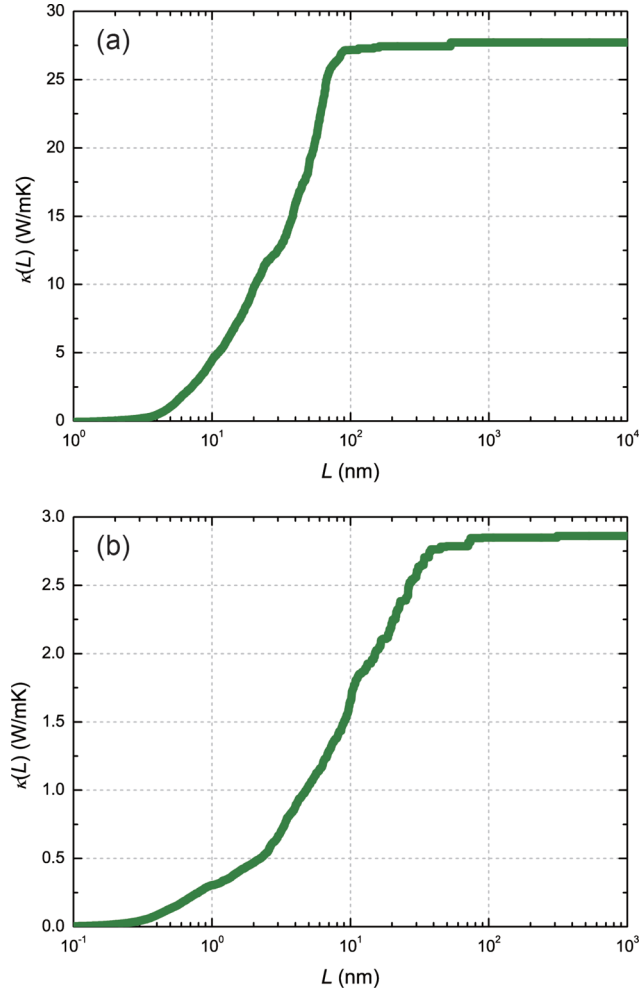

Figure 7. Cumulative thermal conductivity for (a) LB and (b) DB silicene.

noticed that $\tau_j(\mathbf{q})^{anh}$ of LB silicene is much longer than that of DB silicene, leading to much higher lattice thermal conductivity. For DB silicene in Figure 6b, the enhancement of acoustic phonon scattering (corresponding to shorter relaxation time) is the main factor for the reduced lattice thermal conductivity. Moreover, the relaxation times of TA phonons in DB silicene are longer than ZA and LA phonons in the frequency range of 10−80 cm^{-1}. Therefore, the contribution of TA phonons to κ_{nat} of DB silicene is largest (34.43%), as shown in Table 3.

3.3. Size Dependence of κ. With ultralow lattice thermal conductivity, DB silicene may realize higher TE efficiency. This will motivate a systematic examination of the size dependence of thermal conductivity in these two materials for TE applications. To analyze the size dependence of thermal conductivity, we calculate the cumulative thermal conductivity with mean free path (MFP) below L by the following expression

$$\kappa(L) = \kappa_{\alpha\alpha}(L) = \frac{1}{V}\sum_{\lambda}^{l_\lambda<L} C_\lambda v_{\lambda\alpha}^2 \tau_{\lambda\alpha} \tag{8}$$

The cumulative thermal conductivity at 300 K with respect to L for LB and DB silicene are shown in Figure 7a, b, respectively. For LB silicene, the accumulation function closely resembles a step function, with the major contribution by phonons with MFP between 5 and 100 nm. For DB silicene, the major contribution comes from phonons with MFP between 0.5 and 100 nm.

Furthermore, when the size of sample gets smaller, the boundary scattering becomes dominant over other scattering mechanisms, and the κ becomes proportional to a constant value l_{SG}, which limits the MFP uniformly.[37] The l_{SG} can be calculated as

$$l_{SG} = \kappa/\kappa_{SG} \tag{9}$$

where κ_{SG} is the thermal conductivity per l_{SG} in the small-grain limit. The l_{SG} at 300 K is found to be 16.76 nm (2.34 nm) for LB (DB) silicene. These quantities are crucial to the manipulation of phonon transport in the small-grain limit such as nanowires.

In both LB and DB silicene nanowires, the κ will be further reduced with decreasing width due to stronger boundary scattering, as shown in Figure 8. At width about 13 and 4 nm for LB and DB silicene respectively, the lattice thermal conductivity drops about 50%, which means that κ of DB silicene is less sensitive to nanostructuring size effects than LB silicene. Actually, higher lattice thermal conductivity arises typically because of weaker intrinsic phonon scattering, which causes phonons to have larger MFPs.[39] Consequently, these long-MFP phonons can be more easily blocked by boundaries of a similar size. Thus, because DB silicene has lower intrinsic

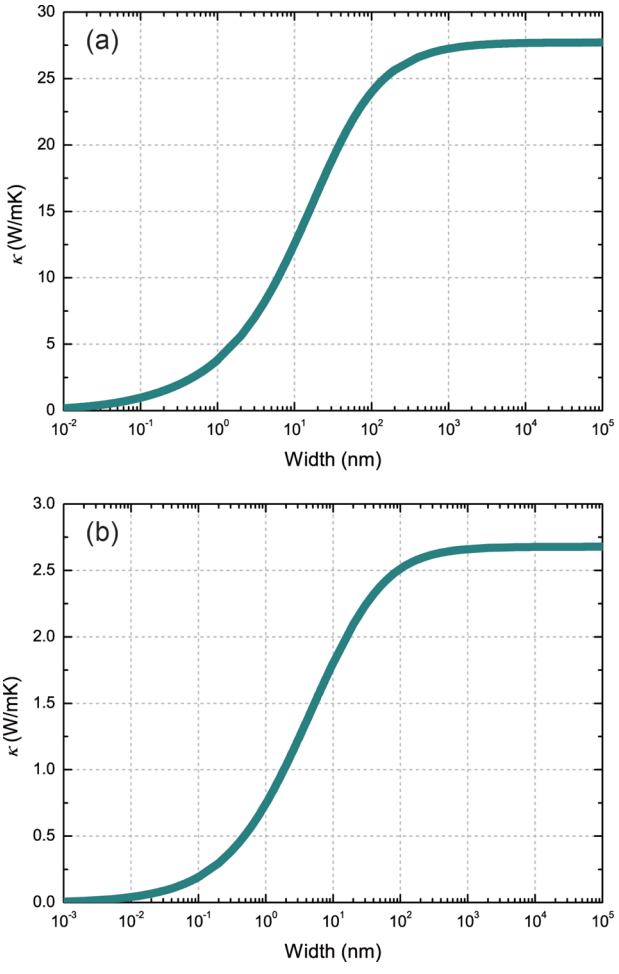

Figure 8. Thermal conductivities of (a) LB and (b) DB silicene nanowires along the [100] direction as a function of width.

thermal conductivity, it is hard to reduce κ further in nanostructures.

4. CONCLUSION

In summary, the lattice thermal conductivity of LB and DB silicene are calculated using first-principles calculations and the BTE for phonons. The κ of both LB and DB silicene are found to be insensitive to naturally occurring isotopes. Much stronger anharmonic phonon scattering is observed in DB silicene as compared with LB silicene. Therefore, the predicted lattice thermal conductivity of DB silicene is much lower than other 2D materials, which will induce further theoretical and experimental investigations on the TE performance for these two structures of silicene. Finally, for designing nanostructures in TE applications, we investigate the size-dependent thermal conductivity in detail.

AUTHOR INFORMATION

Corresponding Authors

*E-mail: zhangh@fudan.edu.cn.
*E-mail: hyzhu@fudan.edu.cn.

Notes

The authors declare no competing financial interest.

ACKNOWLEDGMENTS

This work is supported by the National Basic Research Program of China (973 Program) under Grant 2013CBA01505, and the National Natural Science Foundation of China under Grants 11374063 and 11404348.

REFERENCES

(1) Zhang, Y.; Tan, Y.-W.; Stormer, H. L.; Kim, P. Experimental Observation of the Quantum Hall Effect and Berry's Phase in Graphene. *Nature* **2005**, *438*, 201−204.
(2) Geim, A. K. Graphene: Status and Prospects. *Science* **2009**, *324*, 1530−1534.
(3) Novoselov, K. S.; Fal'ko, V. I.; Colombo, L.; Gellert, P. R.; Schwab, M. G.; Kim, K. A Roadmap for Graphene. *Nature* **2012**, *490*, 192−200.
(4) Klinovaja, J.; Loss, D. Spintronics in MoS_2 Monolayer Quantum Wires. *Phys. Rev. B: Condens. Matter Mater. Phys.* **2013**, *88*, 075404.
(5) Issi, J.-P.; Araujo, P. T.; Dresselhaus, M. S. In *Physics of Graphene*; Aoki, H., Dresselhaus, M. S., Eds.; Springer: New York, 2014; Chapter 3, pp 65−112.
(6) Luican-Mayer, A.; Andrei, E. Y. In *Physics of Graphene*; Aoki, H., Dresselhaus, M. S., Eds.; Springer: New York, 2014; Chapter 2, pp 29−63.
(7) Ferrari, A. C.; Bonaccorso, F.; Fal'ko, V.; Novoselov, K. S.; Roche, S.; Boggild, P.; Borini, S.; Koppens, F. H. L.; Palermo, V.; Pugno, N.; Garrido, J. A.; Sordan, R.; Bianco, A.; Ballerini, L.; Prato, M.; Lidorikis, E.; Kivioja, J.; Marinelli, C.; Ryhanen, T.; Morpurgo, A.; Coleman, J. N.; Nicolosi, V.; Colombo, L.; Fert, A.; Garcia-Hernandez, M.; Bachtold, A.; Schneider, G. F.; Guinea, F.; Dekker, C.; Barbone, M.; Sun, Z.; Galiotis, C.; Grigorenko, A. N.; Konstantatos, G.; Kis, A.; Katsnelson, M.; Vandersypen, L.; Loiseau, A.; Morandi, V.; Neumaier, D.; Treossi, E.; Pellegrini, V.; Polini, M.; Tredicucci, A.; Williams, G. M.; Hee Hong, B.; Ahn, J.-H.; Min Kim, J.; Zirath, H.; van Wees, B. J.; van der Zant, H.; Occhipinti, L.; Di Matteo, A.; Kinloch, I. A.; Seyller, T.; Quesnel, E.; Feng, X.; Teo, K.; Rupesinghe, N.; Hakonen, P.; Neil, S. R. T.; Tannock, Q.; Lofwander, T.; Kinaret, J. Science and Technology Roadmap for Graphene, Related Two-dimensional Crystals, and Hybrid Systems. *Nanoscale* **2015**, *7*, 4598−4810.
(8) Cahangirov, S.; Topsakal, M.; Aktürk, E.; Şahin, H.; Ciraci, S. Two- and One-Dimensional Honeycomb Structures of Silicon and Germanium. *Phys. Rev. Lett.* **2009**, *102*, 236804.
(9) Liu, C.-C.; Feng, W.; Yao, Y. Quantum Spin Hall Effect in Silicene and Two-dimensional Germanium. *Phys. Rev. Lett.* **2011**, *107*, 076802.
(10) Liu, C.-C.; Jiang, H.; Yao, Y. Low-energy Effective Hamiltonian Involving Spin-orbit Coupling in Silicene and Two-dimensional Germanium and Tin. *Phys. Rev. B: Condens. Matter Mater. Phys.* **2011**, *84*, 195430.
(11) Xu, Y.; Yan, B.; Zhang, H.-J.; Wang, J.; Xu, G.; Tang, P.; Duan, W.; Zhang, S.-C. Large-Gap Quantum Spin Hall Insulators in Tin Films. *Phys. Rev. Lett.* **2013**, *111*, 136804.
(12) Xu, Y.; Gan, Z.; Zhang, S.-C. Enhanced Thermoelectric Performance and Anomalous Seebeck Effects in Topological Insulators. *Phys. Rev. Lett.* **2014**, *112*, 226801.
(13) Xu, Y.; Li, Z.; Duan, W. Thermal and Thermoelectric Properties of Graphene. *Small* **2014**, *10*, 2182−2199.
(14) Roome, N. J.; Carey, J. D. Beyond Graphene: Stable Elemental Monolayers of Silicene and Germanene. *ACS Appl. Mater. Interfaces* **2014**, *6*, 7743−7750.
(15) Balendhran, S.; Walia, S.; Nili, H.; Sriram, S.; Bhaskaran, M. Elemental Analogues of Graphene: Silicene, Germanene, Stanene, and Phosphorene. *Small* **2015**, *11*, 640−652.
(16) Matusalem, F.; Marques, M.; Teles, L. K.; Bechstedt, F. Stability and Electronic Structure of Two-dimensional Allotropes of Group-iv Materials. *Phys. Rev. B: Condens. Matter Mater. Phys.* **2015**, *92*, 045436.
(17) Peng, B.; Zhang, H.; Shao, H.; Xu, Y.; Zhang, X.; Zhu, H. Low Lattice Thermal Conductivity of Stanene. *Sci. Rep.* **2016**, *6*, 20225.

(18) Lu, Y. H.; Zhou, D.; Wang, T.; Yang, S. A.; Jiang, J. Z. Topological Properties of Atomic Lead Film with Honeycomb Structure. *Sci. Rep.* **2016**, *6*, 21723.
(19) Vogt, P.; De Padova, P.; Quaresima, C.; Avila, J.; Frantzeskakis, E.; Asensio, M. C.; Resta, A.; Ealet, B.; Le Lay, G. Silicene: Compelling Experimental Evidence for Graphenelike Two-Dimensional Silicon. *Phys. Rev. Lett.* **2012**, *108*, 155501.
(20) Dávila, M. E.; Xian, L.; Cahangirov, S.; Rubio, A.; Le Lay, G. Germanene: a Novel Two-dimensional Germanium Allotrope Akin to Graphene and Silicene. *New J. Phys.* **2014**, *16*, 095002.
(21) Zhu, F.-f.; Chen, W.-j.; Xu, Y.; Gao, C.-l.; Guan, D.-d.; Liu, C.-h.; Qian, D.; Zhang, S.-C.; Jia, J.-f. Epitaxial Growth of Two-dimensional Stanene. *Nat. Mater.* **2015**, *14*, 1020−1025.
(22) Kaltsas, D.; Tsetseris, L. Stability and Electronic Properties of Ultrathin Films of Silicon and Germanium. *Phys. Chem. Chem. Phys.* **2013**, *15*, 9710−9715.
(23) Cahangirov, S.; Özçelik, V. O.; Rubio, A.; Ciraci, S. Silicite: the Layered Allotrope of Silicon. *Phys. Rev. B: Condens. Matter Mater. Phys.* **2014**, *90*, 085426.
(24) Özçelik, V. O.; Kecik, D.; Durgun, E.; Ciraci, S. Adsorption of Group IV Elements on Graphene, Silicene, Germanene, and Stanene: Dumbbell Formation. *J. Phys. Chem. C* **2015**, *119*, 845−853.
(25) Özçelik, V. O.; Gurel, H. H.; Ciraci, S. Self-healing of Vacancy Defects in Single-layer Graphene and Silicene. *Phys. Rev. B: Condens. Matter Mater. Phys.* **2013**, *88*, 045440.
(26) Özçelik, V. O.; Ciraci, S. Local Reconstructions of Silicene Induced by Adatoms. *J. Phys. Chem. C* **2013**, *117*, 26305−26315.
(27) Cahangirov, S.; Özçelik, V. O.; Xian, L.; Avila, J.; Cho, S.; Asensio, M. C.; Ciraci, S.; Rubio, A. Atomic Structure of the $\sqrt{3}\times\sqrt{3}$ Phase of Silicene on Ag(111). *Phys. Rev. B: Condens. Matter Mater. Phys.* **2014**, *90*, 035448.
(28) Tang, P.; Chen, P.; Cao, W.; Huang, H.; Cahangirov, S.; Xian, L.; Xu, Y.; Zhang, S.-C.; Duan, W.; Rubio, A. Stable Two-dimensional Dumbbell Stanene: a Quantum Spin Hall Insulator. *Phys. Rev. B: Condens. Matter Mater. Phys.* **2014**, *90*, 121408.
(29) Özçelik, V. O.; Durgun, E.; Ciraci, S. New Phases of Germanene. *J. Phys. Chem. Lett.* **2014**, *5*, 2694−2699.
(30) Chen, X.; Li, L.; Zhao, M. Hydrogenation-induced Large-gap Quantum-spin-hall Insulator States in a Germanium-tin Dumbbell Structure. *RSC Adv.* **2015**, *5*, 72462−72468.
(31) Qin, G.; Yan, Q.-B.; Qin, Z.; Yue, S.-Y.; Cui, H.-J.; Zheng, Q.-R.; Su, G. Hinge-like Structure Induced Unusual Properties of Black Phosphorus and New Strategies to Improve the Thermoelectric Performance. *Sci. Rep.* **2014**, *4*, 6946.
(32) Fan, Z.; Zheng, J.; Wang, H.-Q.; Zheng, J.-C. Enhanced Thermoelectric Performance in Three-dimensional Superlattice of Topological Insulator Thin Films. *Nanoscale Res. Lett.* **2012**, *7*, 570.
(33) Slack, G. A. Nonmetallic Crystals with High Thermal Conductivity. *J. Phys. Chem. Solids* **1973**, *34*, 321−335.
(34) Shao, H.; Tan, X.; Hu, T.; Liu, G.-Q.; Jiang, J.; Jiang, H. First-principles Study on the Lattice Dynamics and Thermodynamic Properties of Cu_2gese_3. *EPL (Europhysics Letters)* **2015**, *109*, 47004.
(35) Peng, B.; Zhang, H.; Shao, H.; Xu, Y.; Zhang, X.; Zhu, H. Thermal Conductivity of Monolayer Mos_2, $Mose_2$, and Ws_2: Interplay of Mass Effect, Interatomic Bonding and Anharmonicity. *RSC Adv.* **2016**, *6*, 5767−5773.
(36) Omini, M.; Sparavigna, A. Beyond the Isotropic-model Approximation in the Theory of Thermal Conductivity. *Phys. Rev. B: Condens. Matter Mater. Phys.* **1996**, *53*, 9064−9073.
(37) Li, W.; Carrete, J.; Katcho, N. A.; Mingo, N. Shengbte: a Solver of the Boltzmann Transport Equation for Phonons. *Comput. Phys. Commun.* **2014**, *185*, 1747−1758.
(38) Li, W.; Mingo, N.; Lindsay, L.; Broido, D. A.; Stewart, D. A.; Katcho, N. A. Thermal Conductivity of Diamond Nanowires from First Principles. *Phys. Rev. B: Condens. Matter Mater. Phys.* **2012**, *85*, 195436.
(39) Li, W.; Lindsay, L.; Broido, D. A.; Stewart, D. A.; Mingo, N. Thermal Conductivity of Bulk and Nanowire $Mg_2si_xsn_{1-x}$ Alloys from First Principles. *Phys. Rev. B: Condens. Matter Mater. Phys.* **2012**, *86*, 174307.
(40) Li, W.; Carrete, J.; Mingo, N. Thermal Conductivity and Phonon Linewidths of Monolayer Mos_2 from First Principles. *Appl. Phys. Lett.* **2013**, *103*, 253103.
(41) Ouyang, T.; Hu, M. Competing Mechanism Driving Diverse Pressure Dependence of Thermal Conductivity of *x*te (*x* = hg, cd, and zn). *Phys. Rev. B: Condens. Matter Mater. Phys.* **2015**, *92*, 235204.
(42) Hu, M.; Zhang, X.; Poulikakos, D. Anomalous Thermal Response of Silicene to Uniaxial Stretching. *Phys. Rev. B: Condens. Matter Mater. Phys.* **2013**, *87*, 195417.
(43) Kuang, Y. D.; Lindsay, L.; Shi, S. Q.; Zheng, G. P. Tensile Strains Give Rise to Strong Size Effects for Thermal Conductivities of Silicene, Germanene and Stanene. *Nanoscale* **2016**, *8*, 3760−3767.
(44) Kresse, G.; Furthmüller, J. Efficient Iterative Schemes for *ab Initio* Total-energy Calculations Using a Plane-wave Basis Set. *Phys. Rev. B: Condens. Matter Mater. Phys.* **1996**, *54*, 11169−11186.
(45) Baroni, S.; de Gironcoli, S.; Dal Corso, A.; Giannozzi, P. Phonons and Related Crystal Properties from Density-functional Perturbation Theory. *Rev. Mod. Phys.* **2001**, *73*, 515−562.
(46) Drummond, N. D.; Zólyomi, V.; Fal'ko, V. I. Electrically Tunable Band Gap in Silicene. *Phys. Rev. B: Condens. Matter Mater. Phys.* **2012**, *85*, 075423.
(47) Scalise, E.; Houssa, M.; Pourtois, G.; van den Broek, B.; Afanas'ev, V.; Stesmans, A. Vibrational Properties of Silicene and Germanene. *Nano Res.* **2013**, *6*, 19−28.
(48) Gu, X.; Yang, R. First-principles Prediction of Phononic Thermal Conductivity of Silicene: a Comparison with Graphene. *J. Appl. Phys.* **2015**, *117*, 025102.
(49) Huang, L.-F.; Gong, P.-L.; Zeng, Z. Phonon Properties, Thermal Expansion, and Thermomechanics of Silicene and Germanene. *Phys. Rev. B: Condens. Matter Mater. Phys.* **2015**, *91*, 205433.
(50) Li, X.; Mullen, J. T.; Jin, Z.; Borysenko, K. M.; Buongiorno Nardelli, M.; Kim, K. W. Intrinsic Electrical Transport Properties of Monolayer Silicene and Mos_2 from First Principles. *Phys. Rev. B: Condens. Matter Mater. Phys.* **2013**, *87*, 115418.
(51) Peng, B.; Zhang, H.; Shao, H.; Xu, Y.; Zhang, R.; Zhu, H. ab Initio Study of Phonon-transport Properties of Two-dimensional Group-iv Materials. *arXiv*, **2016**, 1602.02266v1.
(52) Efetov, D. K.; Kim, P. Controlling Electron-Phonon Interactions in Graphene at Ultrahigh Carrier Densities. *Phys. Rev. Lett.* **2010**, *105*, 256805.
(53) Tohei, T.; Kuwabara, A.; Oba, F.; Tanaka, I. Debye Temperature and Stiffness of Carbon and Boron Nitride Polymorphs from First Principles Calculations. *Phys. Rev. B: Condens. Matter Mater. Phys.* **2006**, *73*, 064304.
(54) Shao, H.; Tan, X.; Jiang, J.; Jiang, H. First-principles Study on the Elastic Properties of Cu_2gese_3. *EPL (Europhysics Letters)* **2016**, *113*, 26001.
(55) Nakashima, T.; Umakoshi, Y. Anisotropy of Electrical Resistivity and Thermal Expansion of Single-crystal Ti_5si_3. *Philos. Mag. Lett.* **1992**, *66*, 317−321.
(56) Lindsay, L.; Broido, D. A.; Reinecke, T. L. First-Principles Determination of Ultrahigh Thermal Conductivity of Boron Arsenide: A Competitor for Diamond? *Phys. Rev. Lett.* **2013**, *111*, 025901.
(57) Shao, H.; Tan, X.; Liu, G.-Q.; Jiang, J.; Jiang, H. A First-principles Study on the Phonon Transport in Layered Bicuose. *Sci. Rep.* **2016**, *6*, 21035.
(58) Li, H.-P.; Zhang, R.-Q. Vacancy-defect-induced Diminution of Thermal Conductivity in Silicene. *EPL (Europhysics Letters)* **2012**, *99*, 36001.
(59) Pei, Q.-X.; Zhang, Y.-W.; Sha, Z.-D.; Shenoy, V. B. Tuning the Thermal Conductivity of Silicene with Tensile Strain and Isotopic Doping: a Molecular Dynamics Study. *J. Appl. Phys.* **2013**, *114*, 033526.
(60) Xie, H.; Ouyang, T.; Germaneau, E.; Qin, G.; Hu, M.; Bao, H. Large Tunability of Lattice Thermal Conductivity of Monolayer Silicene Via Mechanical Strain. *Phys. Rev. B: Condens. Matter Mater. Phys.* **2016**, *93*, 075404.

(61) Wang, Z.; Feng, T.; Ruan, X. Thermal Conductivity and Spectral Phonon Properties of Freestanding and Supported Silicene. *J. Appl. Phys.* **2015**, *117*, 084317.
(62) Zhang, X.; Bao, H.; Hu, M. Bilateral Substrate Effect on the Thermal Conductivity of Two-dimensional Silicon. *Nanoscale* **2015**, *7*, 6014−6022.
(63) Ziman, J. M. *Electrons and Phonons: The Theory of Transport Phenomena in Solids*; Oxford University Press: Oxford, 1960.
(64) Grimvall, G. *Thermophysical Properties of Materials*; Elsevier Science: Amsterdam, 1999.
(65) Fugallo, G.; Lazzeri, M.; Paulatto, L.; Mauri, F. *ab Initio* Variational Approach for Evaluating Lattice Thermal Conductivity. *Phys. Rev. B: Condens. Matter Mater. Phys.* **2013**, *88*, 045430.
(66) Akhmedova, G. A.; Abdinov, D. S. Effect of Thallium Doping on the Thermal Conductivity of Pbte Single Crystals. *Inorg. Mater.* **2009**, *45*, 854−858.
(67) Yan, R.; Simpson, J. R.; Bertolazzi, S.; Brivio, J.; Watson, M.; Wu, X.; Kis, A.; Luo, T.; Hight Walker, A. R.; Xing, H. G. Thermal Conductivity of Monolayer Molybdenum Disulfide Obtained from Temperature-Dependent Raman Spectroscopy. *ACS Nano* **2014**, *8*, 986−993.
(68) Zhang, X.; Sun, D.; Li, Y.; Lee, G.-H.; Cui, X.; Chenet, D.; You, Y.; Heinz, T. F.; Hone, J. C. Measurement of Lateral and Interfacial Thermal Conductivity of Single- and Bilayer MoS_2 and $MoSe_2$ Using Refined Optothermal Raman Technique. *ACS Appl. Mater. Interfaces* **2015**, *7*, 25923−25929.
(69) Peng, B.; Zhang, H.; Shao, H.; Xu, Y.; Zhang, X.; Zhu, H. Towards Intrinsic Phonon Transport In Single-layer Mos_2. *Ann. Phys.* **2016**, *528*, 504−511.
(70) Jain, A.; McGaughey, A. J. H. Strongly Anisotropic In-plane Thermal Transport in Single-layer Black Phosphorene. *Sci. Rep.* **2015**, *5*, 8501.
(71) Balandin, A. A.; Ghosh, S.; Bao, W.; Calizo, I.; Teweldebrhan, D.; Miao, F.; Lau, C. N. Superior Thermal Conductivity of Single-Layer Graphene. *Nano Lett.* **2008**, *8*, 902−907.
(72) Lindsay, L.; Broido, D. A. Three-phonon Phase Space and Lattice Thermal Conductivity in Semiconductors. *J. Phys.: Condens. Matter* **2008**, *20*, 165209.
(73) Wu, X.; Varshney, V.; Lee, J.; Zhang, T.; Wohlwend, J. L.; Roy, A. K.; Luo, T. Hydrogenation of Penta-Graphene Leads to Unexpected Large Improvement in Thermal Conductivity. *Nano Lett.* **2016**, *16*, 3925.
(74) Ziman, J. The Thermal Properties of Materials. *Sci. Am.* **1967**, *217*, 180−188.
(75) Han, Y.; Dong, J.; Qin, J.; Hu, M. Phonon Transport in the Ground State of Two-dimensional Silicon and Germanium. *RSC Adv.* **2016**, *6*, 69956−69965.

NOTE ADDED IN PROOF

We have recently become aware of a related work.[75]